Scientific Research Publishing

Advances in Materials Physics and Chemistry, 2022, 12, 306-322
https://www.scirp.org/journal/ampc
ISSN Online: 2162-5328
ISSN Print: 2162-531X

Microwave-Assisted Hydrolysis of Hemicellulose over Sulfonated Catalysts

Itidel Belkadhi[1], Mohamed Achraf Bouabdellah[1], Lassâad Ben Hammouda[1], Zouhaier Ksibi[1], Francesco Medina[2]

[1]University Tunis-El Manar, Tunisia
[2]Rovira I Virgili University, Tarragona, Spain
Email: itidel.belkadhi@fst.utm.tn

How to cite this paper: Belkadhi, I., Bouabdellah, M.A., Hammouda, L.B., Ksibi, Z. and Medina, F. (2022) Microwave-Assisted Hydrolysis of Hemicellulose over Sulfonated Catalysts. *Advances in Materials Physics and Chemistry*, **12**, 306-322.
https://doi.org/10.4236/ampc.2022.1211020

Received: October 13, 2022
Accepted: November 26, 2022
Published: November 29, 2022

Abstract

Sulfonated catalysts based on zirconia (SO_3H-ZrO_2), silica (SO_3H-SBA-15) and zeolite (SO_3H-ZSM-5) were studied in the catalytic hydrolysis reaction of hemicellulose in a microwave reactor. The prepared catalysts were characterized by various techniques (XRD, N_2 physisorption at 77 K, SEM, TEM and NH_3-TPD). The obtained results reveal that despite the differences in their structural and textural properties, the ZrO_2, Al-SBA-15 and H-ZSM-5 supports show similar conversions. Doping supports with sulfonate species created hydrogen bonds between SO_3H groups and increased the amount of weak acid sites, which enhanced the hydrolysis of hemicellulose. SO_3H-ZSM-5 showed the highest catalytic activity followed by SO_3H-SBA-15 while SO_3H-ZrO_2 exhibited a poor conversion. Furthermore, the catalytic hydrolysis of the hemicellulose leads to several interesting products, such as formic acid, acetic acid, lactic acid and xylan. The correlation between the catalytic performances and the acidic properties of the different samples indicates that the best catalytic performances were obtained with the least acidic solids and especially when the density of strong acid sites decreases.

Keywords

ZrO_2, Al-SBA-15, H-ZSM-5, SO_3H, Hemicellulose, Microwave

1. Introduction

Nowadays, the economic growth as well as the industrialization dramatically increases fuel consumption leading to environmental problems and a decrease in reserves, which requires the use of alternative resources. Decidedly, renewable resources, mainly biomass, are fundamental to satisfy future generations [1]. In

addition to being non-toxic, biodiesels do not contain aromatic or sulfurous compounds, making them "cleaner" fuels than fossil sources. Indeed, they have a higher flammability point, a high cetane number, a negligible concentration of sulfide and a good lubricating efficiency [2]. Lignocellulosic biomass consists of carbohydrates polymers of cellulose, hemicellulose and lignin, which belong to the family of polymeric macromolecules and are the main constituents of wood [3]. In addition, lignocellulosic biomass is diverse and comes from agricultural waste, household waste, and industrial waste. It has a better environmental balance because its water and fertilizer consumption is not important.

The hydrolysis of these polymers is essential to produce various beneficial chemical products [4]. However, these products are not yet fully exploited in the industry. On the other hand, different hemicellulose transformation pathways are used to obtain these chemical products, including the hydrolysis. Several research works have focused on enzymatic hydrolysis [5] [6]. Other works aim the catalytic hydrolysis of hemicellulose using liquid acids such as maleic acid [7] [8], sulfuric acid [9] or even superacid SO_4H-functionalized ionic liquids [10]. To replace costly enzymes and facilitate the separation of the catalysts from the reaction medium, research have resorted to heterogeneous catalysis in the hydrolysis reaction. This represents a great benefit to the industry. Indeed, works on the hemicellulose hydrolysis with solid catalysts are carried out, including acid carbon-based catalyst [11], sulfonated silica gels [12], sulfated zirconia [13] or silica-magnetite nanocomposites [14].

The microwave technique significantly improves the reaction rate as well as the convection of thermal energy and irradiation. It also shows a positive influence on the chemical reaction, by non-thermal effect, which is a unique phenomenon of the heating of microwave radiation. The two basic principles of microwave heating are dipole rotation and ion conduction. Compared to conventional heating, the microwave oven has an advantage for large-scale industrial technologies. Indeed, it constitutes a fast, very efficient and selective process since only the polar materials are directly heated [15] [16]. Several research works are interested in improving the conversion of hemicellulose, using microwave reactors [16] [17]. In our case, we have chosen to use this processing technique because it has proven its worth for organic synthesis [18] or polymer processing [19]. However, no results related to hemicellulose hydrolysis using catalysts based on ZrO_2, Al-SBA-15 and H-ZSM-5 have been reported, even in the absence of a microwave reactor. Indeed, X. Wang *et al.* have studied the conversion of dilute-oxalic acid pretreated bagasse hydrolysate using recyclable ironic phosphates ($FePO_4$) catalyst [20] and Sn-MMT/SO_4^{2-} solid acids as catalysts was used in the biphasic system in a hydrothermal treatment of bagasse [21]. Other studies have focused on the dehydration of d-xylose to furfural using arenesulfonic SBA-15 catalysts [22]. J. Zhang *et al.* were interested in the study of the conversion of D-xylose with MCM-41 as catalyst and butanol as the extraction phase [23]. However, further work has been done to investigate the ef-

fect of microwave-assisted furfural production from xylose and bamboo hemicellulose in a biphasic medium [24]. Results of the hydrolysis of corncob hemicellulose by sulfated zirconia and its evaluation in xylitol production were announced by L. Wan *et al.* [13]. This promoted us to study the hemicellulose hydrolysis reaction in a microwave reactor and to compare the catalytic performances of sulfonated catalysts based on ZrO_2, Al-SBA-15 and H-ZSM-5.

The present work focuses on the optimization of the heterogeneous hydrolysis reaction of hemicellulose assisted by a micro-wave reactor. It also aims to study the influence of the acidity of the different supports modified by sulfonate species on their catalytic performances. Moreover, the by-products obtained by the hydrolysis of hemicellulose which can be used as substrates for the synthesis of several bio-chemical products are studied. The structural and textural properties of the different catalysts were characterized by several techniques (XRD, N_2-physisorption, H_2-TPR, ESEM, TEM, NH_3-TPD) in order to establish a relationship between the physicochemical properties of the catalysts and their catalytic performance in the hydrolysis reaction of hemicellulose.

2. Experimental

2.1. Catalyst Preparation

Zirconia support was prepared by sol-gel process using zirconium propoxide $Zr(OPr)_4$ (Sigma Aldrich 70% in 1-propanol) which was dissolved in 1-propanol. The mixture was stirred for 30 min before adding nitric acid. After 30 min of additional stirring, an adequate amount of deionized water was added to ensure the hydrolysis, with a hydrolysis ratio $nH_2O/nZr = 1$. After the gelation process, the obtained alcogel was dried in an autoclave, under supercritical conditions of the solvent (536 K and 51.7 bar). In order to eliminate the organic residues remaining in the aerogel and convert zirconium hydroxide into zirconium oxide, a calcination process was carried out at 823 K under an oxygen flow (30 $cm^3 \cdot min^{-1}$) during 5 h with a temperature rise of 1 K min^{-1}.

The Al-SBA-15 was prepared by mixing Pluronic 123 (P123, Sigma Aldrich) and 2 M HCl solution and stirred for 15 h at room temperature. The obtained solution was heated up to 40˚C and tetraethyl orthosilicate (TEOS, Aldrich 98%) was added. After 4 h of stirring, aluminum sulphate $Al_2(SO_4)_3 \cdot 18H_2O$ (Aldrich, 98%) was added and followed by 20 h of stirring. The obtained solution was transferred to a Teflon-lined autoclave for a hydrothermal treatment at 100˚C for 48 h. Then, it was cooled at the room temperature to adjust the pH to 7.5, using a concentrated ammonium hydroxide solution, followed by a second hydrothermal treatment in the same conditions. Finally, the obtained product was washed using deionized water and filtrated [25]. The powder was calcined at 823 K under an oxygen flow (30 $cm^3 \cdot min^{-1}$) for 5 h with a temperature rise of 1 K min^{-1}. H-ZSM-5 zeolite (Si/Al = 15) was supplied from Zeolyst International.

The different catalysts were prepared by wet impregnation method. In fact, an adequate amount of 5-sulfoisophtaltalic acid sodium salt $NaO_3SC_6H_3$-1,3-$(CO_2H)_2$

(Aldrich, 95%) was dissolved in deionized water and then each support was mixed with the prepared solution and stirred for 4 h, before drying at 100˚C for 20 hours. Finally, the obtained solids were calcined at 823 K under an oxygen flow (30 $cm^3 \cdot min^{-1}$) for 5 h with a temperature rise of 1 K min^{-1}. The catalysts were donated as follow: SO_3H-ZrO_2, SO_3H-SBA-15, SO_3H-ZSM-5.

2.2. Catalyst Characterization Techniques

The specific surface area, the average pore size and the pore volume were determined using N_2 adsorption-desorption isotherms at 77 K which were performed with a Micrometrics ASAP 2020 apparatus after an outgassing at 473 K for 3 h. The specific surface area and the pore size distribution were determined using BET and BJH methods, respectively.

The temperature programmed desorption of ammonia (NH_3-TPD) was established with an Autochem 2920 apparatus (Micromeritics, USA) equipped with a thermal conductivity detector for gas analysis. Each sample was pretreated at a temperature rise of 20 K min^{-1}, from room temperature up to 873 K, under helium flow (30 $mL \cdot min^{-1}$) for 30 min. Then, the catalyst was cooled down until 323 K and saturated with 5 vol. % NH_3/Ar during 60 min. The physically adsorbed ammonia was desorbed from the sample under a helium flow of 30 $mL \cdot min^{-1}$ for 30 min. The desorption of chemically adsorbed ammonia was registered by increasing temperature from 323 K up to 873 K with a rise of 20 K min^{-1}. GRAMS/32 software was used to calculate the number of acid sites (mmol), by integrating the areas under the desorption peaks. The calculated amount of acid sites ($mmol \cdot g^{-1}$) was normalized by the catalysts weight. In addition, the density of the acid sites is the ratio between the amount of acid sites and the specific surface area of the solid ($mmol \cdot m^{-2}$) [26].

Powder XRD patterns were recorded by a Bruker D8 Siemens EM-10110BU D5000 Diffractometer, using a CuK_α radiation (λ = 1.54060 Å). Diffractograms were recorded between 0.5˚ and 5˚ (2θ) with a step of 0.02˚ in the case of Al-SBA-15 support and between 5˚ and 70˚ for all samples.

Scanning electron microscopy (SEM) images were acquired on a JEOL JSM-6400, operating at an accelerating voltage of 0.4 kV - 40 kV and a resolution of 10 nm.

Transmission electron microscopy (TEM) images were recorded with JEOL JEM-1011 electron microscope. Each sample was suspended and dispersed by ultrasonic treatment in ethanol. A drop of the fine suspension was placed on a copper TEM grid which was loaded into the microscope.

2.3. Catalytic Activity

To study their catalytic properties, the different samples were tested under the same conditions in the hydrolysis reaction of hemicellulose, using a microwaves reactor (MA167-002-SynthWAVE). Before proceeding with the catalytic test, hemicellulose is milled and then sieved to obtain a homogeneous particle size of

100 μm. First, 100 mg of the catalyst and 100 mg of hemicellulose were introduced in a reactor containing 20 mL of deionized water. The temperature was set at 433 K and the pressure was fixed at 10 bar. Hemicellulose conversion was evaluated after 30 min, 1 h or 2 h of reaction. Then, the obtained liquid fraction that was separated from the solid fraction using a vacuum filtration, was analyzed by HPLC (HPLC Agilent tech, 1100 series) with ICSep ICE-COREGEL 87H3 as column, using DAD (measuring at 210 nm) and RID detectors. The mobile phase is an aqueous sulfuric acid solution whose pH is adjusted to 2.2. The HPLC column temperature is fixed at 323 K and the mobile phase flow at 0.6 $mL{\cdot}min^{-1}$. Commercial arabinose, mannose, xylose, levulinic acid, formic acid and furfural were used as standards for the calibration and the qualification of obtained products.

3. Results and Discussion

3.1. Catalyst Characterization

3.1.1. N_2 Physisorption at 77 K

According to IUPAC classification, the N_2 adsorption-desorption isotherms of the synthesized samples were type IV characterized by a very gradual increase in the adsorbed quantity at low relative pressure. For relatively high pressures, they are characterized by a saturation stage, reduced to an inflection point in the case of ZrO_2, SO_3H-ZrO_2, Al-SBA-15 and SO_3H-SBA-15 samples. This type of adsorption isotherm is obtained with mesoporous adsorbents in which capillary condensation occurs. (**Figure 1**)

Prepared samples also showed different types of hysteresis. The main type was H3, which is related to split-shaped pores formed by non-rigid plate aggregates. This type of hysteresis corresponds to particles in the form of platelets or leaflets swelling under the effect of condensation in the mesopores. The pore size distribution curves determined by BJH method reveal that the catalysts based on zirconia shows a relatively homogeneous pore size distribution. The pore size of ZrO_2 is centered at 439Å and that of SO_3H-ZrO_2 at 150 Å. Furthermore, the pore size distribution of Al-SBA-15 and SO_3H-SBA-15 samples is bimodal. Indeed, it is centered at 174 Å and 439 Å for the first one, and at 70 Å and 874 Å for its sulfonated counterpart. It should be noted that H-ZSM-5 and SO_3H-ZSM-5 samples exhibit a heterogeneous pore size distribution with different pores diameter situated between 20 Å and 430 Å.

Other textural properties of synthesized samples are listed in **Table 1**. The specific surface areas for obtained samples ranged from 90 to 404 $m^2{\cdot}g^{-1}$, the average pore diameter from 80 to 234 Å and the pore volume from 0.10 to 1.19 $cm^3{\cdot}g^{-1}$. The comparative study between the textural properties of the supports and their sulfonated counterparts indicates that the incorporation of the sulfonate groups leads to a significant decrease in the specific surface area and the pore volume, especially for the Al-SBA-15 sample, whose surface area drops by 71%. This result may be explained by the clogging of the pores preventing the

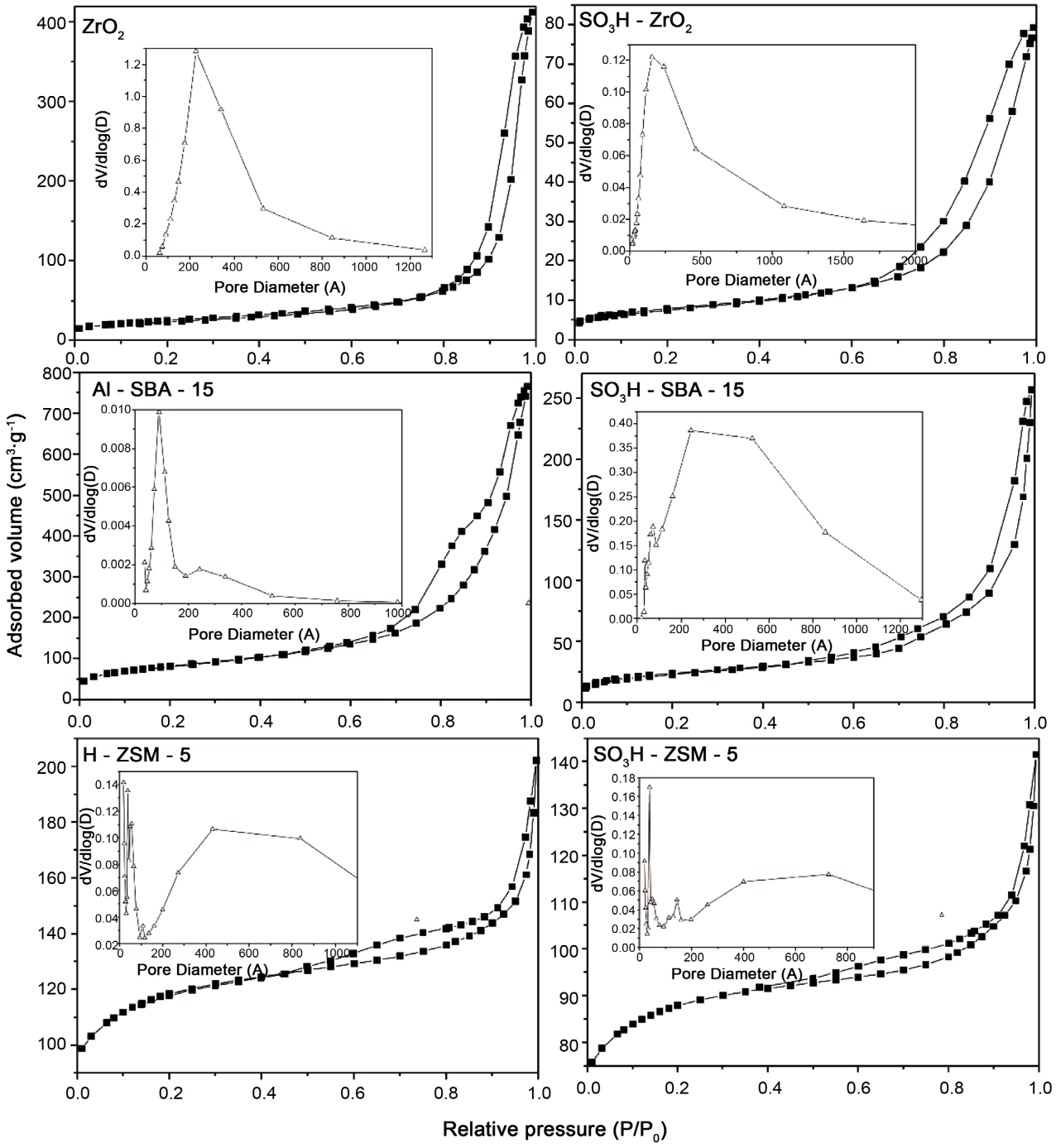

Figure 1. N_2 Adsorption-desorption isotherms and pore size distribution of the catalysts.

access of nitrogen molecules in the letter. The preparation method has also a great influence on the textural properties of the catalysts.

3.1.2. XRD Results

Examination of XRD patterns of ZrO_2 and SO_3H-ZrO_2 samples reveals the presence of two crystalline phases of ZrO_2, the metastabletetragonal phase, identified by its most intense characteristic peaks observed at $2\theta = 30^\circ$, 35°, 60° and 65°

Table 1. Textural properties of the catalysts.

Catalysts	S_{BET} (m^2/g)	Average pore diameter (Å)	Pore volume ($cm^3 \cdot g^{-1}$)
ZrO_2	90	234	0.64
SO_3H-ZrO_2	28	127	0.12
Al-SBA-15	813	138	1.19
SO_3H-SBA-15	194	165	0.39
H-ZSM-5	404	80	0.16
SO_3H-ZSM-5	298	85	0.10

[27], as well as the stable monoclinic phase characterized by its most intense peaks located at $2\theta = 24^\circ$, 28°, 31° and 50°. However, it seems that the impregnation of the zirconia particles with the SO_3H groups don't have a considerable effect on the crystalline structure of zirconia [28] except that it accelerates the transition from the metastabletetragonal phase to the stable monoclinic one. Indeed, it's noted that the characteristic lines of the monoclinic phase (28° and 31°) become much more intense after sulfonation than those attributed to the tetragonal phase indicating that the interaction between the sulfonate groups and the surface of the support is relatively weak (**Figure 2**).

XRD patterns of Al-SBA-15 and SO_3H-SBA-15 solids show the existence of peaks located at the small angles ($2\theta = 0.9^\circ$ and 1.8°) corresponding to the (100) diffraction plan and indicating an ordered hexagonal mesoporous structure with 8.9 nm channels, which are specific of p6mm symmetry [29] [30]. Furthermore, Al-SBA-15 and SO_3H-SBA-15 XRD patterns reveal the same peaks with the same intensities, which indicate that the mesoporous structure of the Al-SBA-15 is preserved after its modification by the sulfonate species [14]. Otherwise, at high 2θ angles, XRD patterns of SO_3H-SBA-15 mainly show a broad peak centered at 23° (**Figure 3**).

Concerning the H-ZSM-5 support and its sulfonated counterparts, the XRD patterns reveal several peaks. The most intense are observed at 7°, 8°, 23° and 24°. These peaks are characteristic of a highly crystalline orthorhombic MFI type framework of the zeolite [31] [32]. These peaks are located at the same angles on H-ZSM-5 and SO_3H-ZSM-5 catalysts, which indicates that the crystallinity of H-ZSM-5 framework was preserved after its modification with sulfonated groups. Moreover, the peaks intensity of SO_3H-ZSM-5 are slightly weaker than those of pure H-ZSM-5, which is probably due to the removal of the partial extra-amorphous framework of Al on the surface and in H-ZSM-5 channel [33] (**Figure 4**).

3.1.3. SEM Results

The particle morphology of all sulfonated solids was evaluated by scanning electron microscopy (**Figure 5**). SEM micrographs of SO_3H-ZrO_2 and SO_3H-ZSM-5 showed heterogeneous particles. Indeed, the shapes of the particles on the

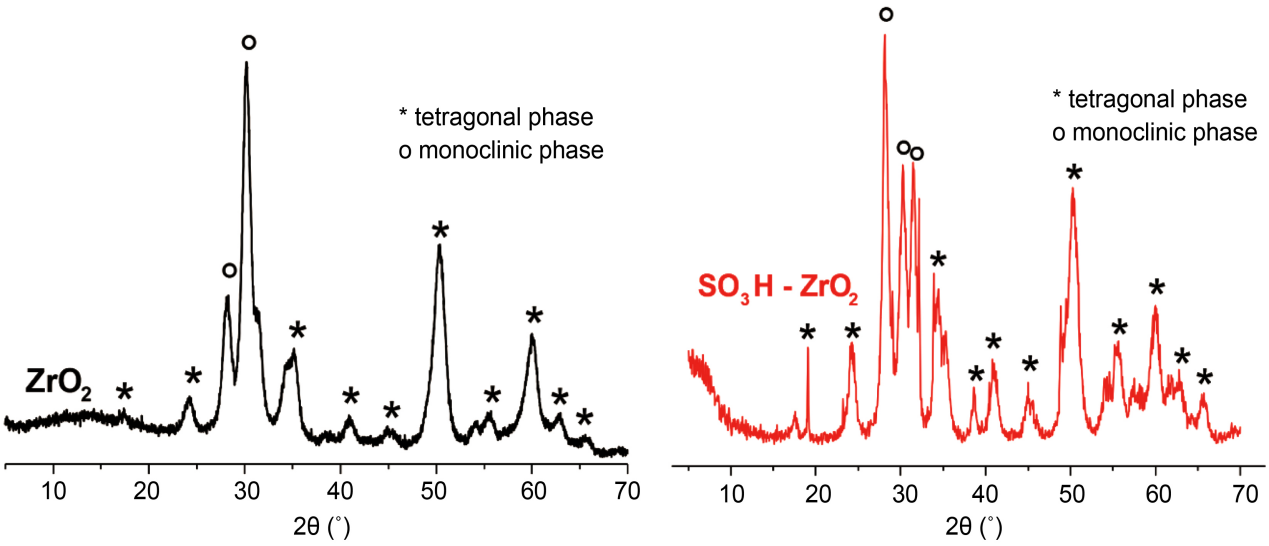

Figure 2. XRD patterns of ZrO_2 and SO_3H-ZrO_2.

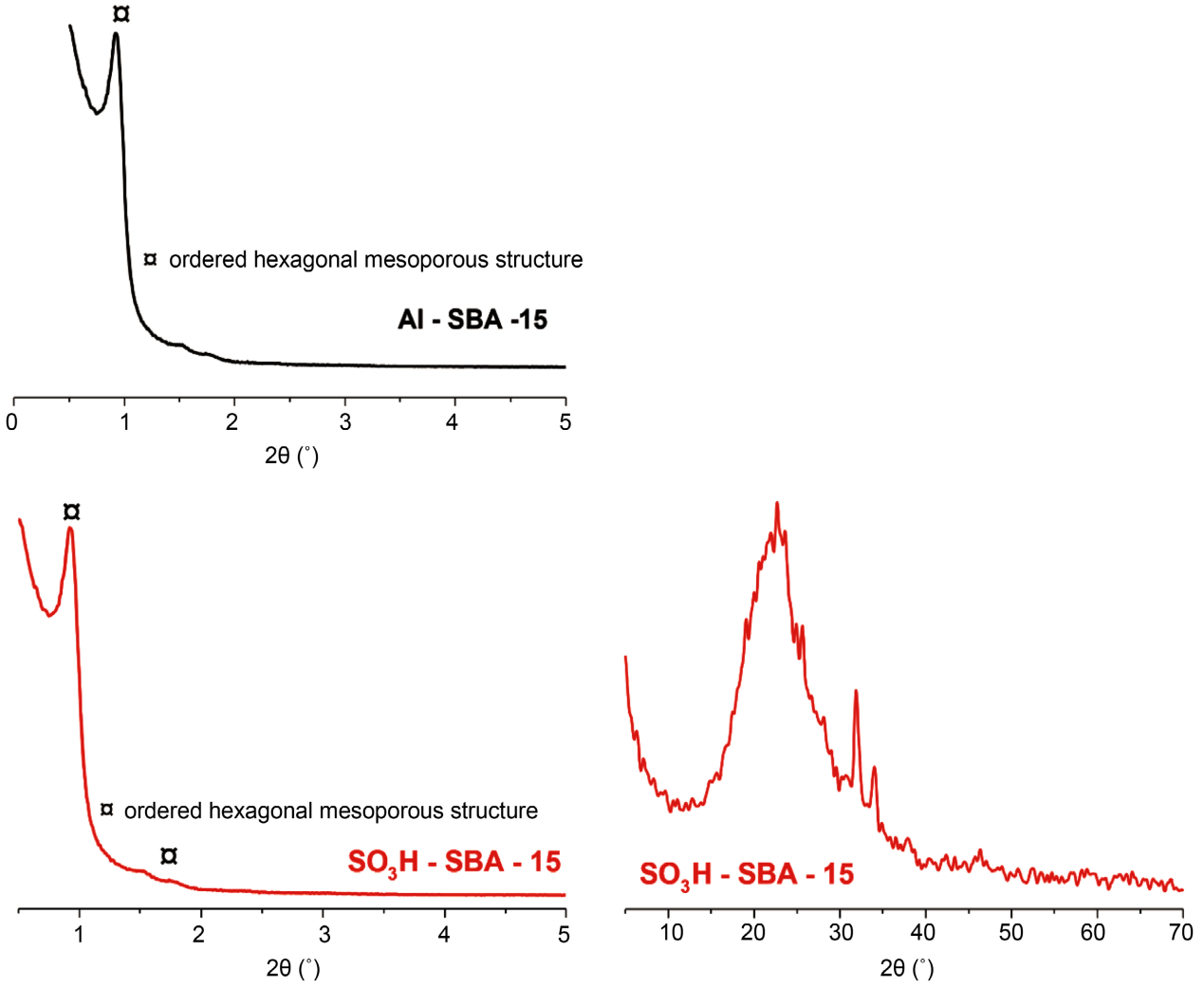

Figure 3. XRD patterns of Al-SBA-15 and SO_3H-SBA-15.

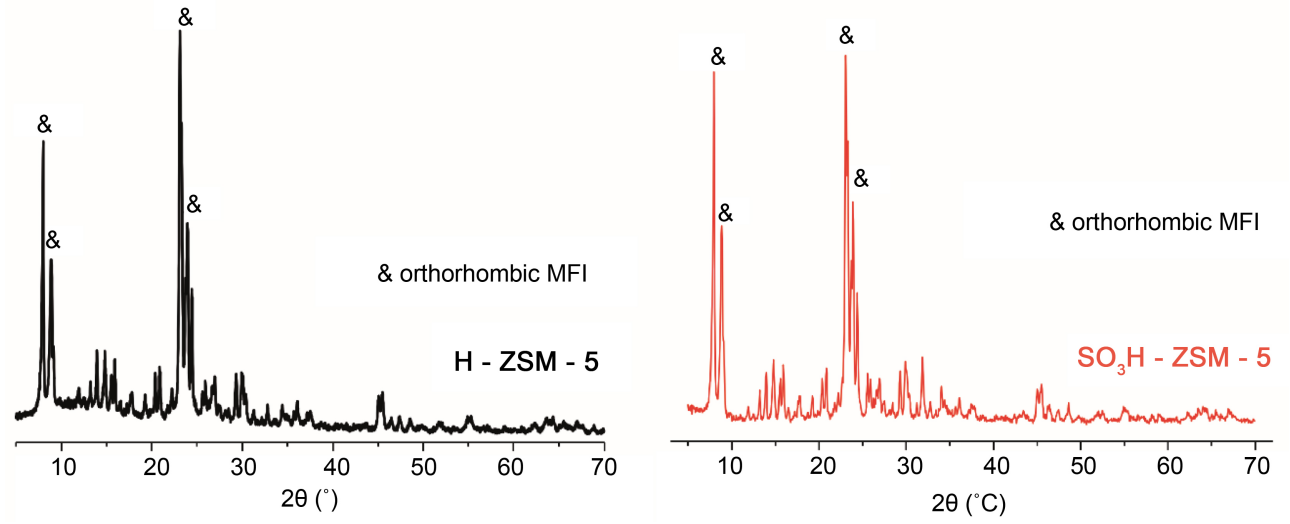

Figure 4. XRD patterns of H-ZSM-5 and SO_3H-ZSM-5.

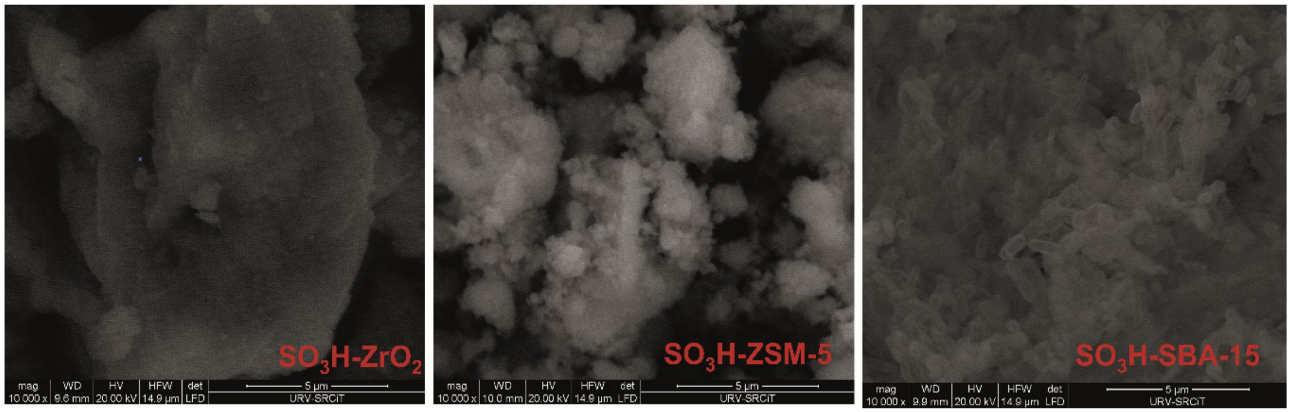

Figure 5. SEM images of the catalysts.

surface are irregular, resulting from the aggregation of the nanoparticles [30]. This aggregation is supported by the presence of the sulfonate groups which contribute to the establishment of hydrogen bonds [34]. Moreover, SEM micrograph of SO_3H-SBA-15 sample showed a certain homogeneity in the shape of the particles which are cylindrical with hexagonal symmetry [29] (**Table 2**).

3.1.4. TEM Results

Transmission electron microscopy image of SO_3H-ZrO_2 showed compact particles with a very heterogeneous size and shape distribution. However, the TEM Image of SO_3H-SBA-15 confirms that the particles are practically uniform in size and are characterized by cylindrical shapes. Furthermore, the TEM micrograph of SO_3H-ZSM-5 sample showed spherical structure particles obtained by aggregation of several nanoparticles having relatively similar shapes (**Figure 6**).

3.1.5. NH_3-TPD Results

The NH_3-TPD was used to characterize the acidity of synthesized samples. Both, the amount of desorbed NH_3 and the desorption temperature allow to estimate

Table 2. EDS analysis of the catalysts.

Sample	Wt% Zr	Wt% Al	Wt% Si	Wt% O	Wt% S
SO_3H-ZrO_2	42.62	---	---	30.11	6.31
SO_3H-SBA-15	---	1.07	33.02	46.99	0.88
SO_3H-ZSM-5	---	1.31	28.61	44.40	1.59

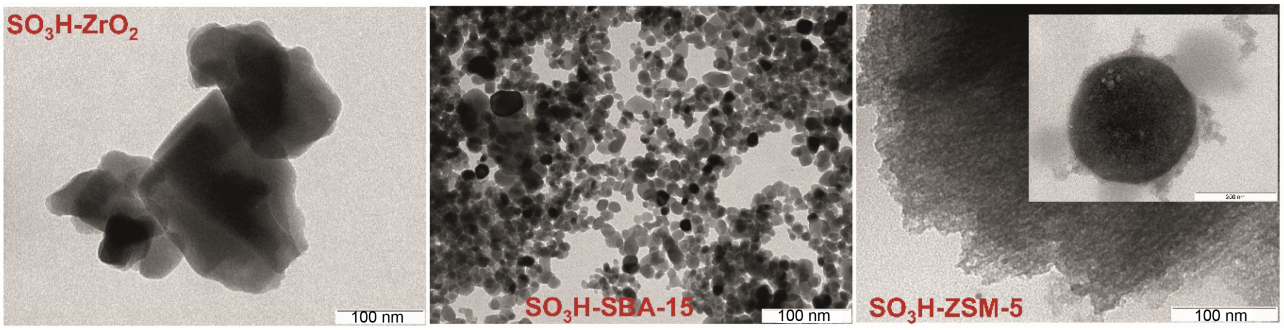

Figure 6. TEM images of the catalysts.

the number of acid sites and their strengths, respectively. Table 3 presents the total acidity as well as the density of acid sites of all obtained solids. The results show that the addition of the sulfonate species relatively increases the total amount of desorbed NH_3 and the density of acid sites in the case of the Al-SBA-15 support. However, the results related to zirconia and H-ZSM-5 reveal that the incorporation of the SO_3H groups induces a decrease of the total acidity. In fact, the amount of desorbed NH_3 drops from 1.90 mmol per gram of ZrO_2 to 0.57 mmol·g^{-1} for SO_3H-ZrO_2 and from 12.75 mmol·g^{-1} for H-ZSM-5 to 6.43 mmol·g^{-1} for SO_3H-ZSM-5 sample. This is also accompanied by a drop in acid sites density for these last two sulfonated samples. According to the literature [35] [36], the desorption peaks obtained at temperatures lower than 200˚C correspond to weak acid sites, while those situated between 200˚C and 350˚C are related to medium acid sites and those occurring at temperatures higher than 400˚C are associated to strong acid sites. The NH_3-TPD curves of the different samples were explored by Gaussian deconvolution function in order to be able to evaluate the distribution of acid sites according to their strength as well as the amount of desorbed NH_3 in each case.

Examination of Figure 7 and Table 3 reveals that only the solids ZrO_2, SO_3H-ZrO_2 and SO_3H-ZSM-5 contain strong acid sites. In addition, sulfonation leads to a great drop in the amount of strong acid sites which disappear completely in the case of the H-ZSM-5 support and decreases from 0.75 mmol·g^{-1} for ZrO_2 to 0.15 mmol·g^{-1} for the sulfonated form SO_3H-ZrO_2. The incorporation of the sulfonate groups also leads to a drop in the medium acidity for the three supports used. Indeed, the quantity of desorbed ammonia corresponding to the acid sites of medium strength shows a significant drop since it goes from 0.78 mmol·g^{-1} for ZrO_2 to 0.20 mmol·g^{-1} for SO_3H-ZrO_2 and from 0.08 mmol·g^{-1} in

Table 3. Quantification and density of acid sites of catalysts.

Catalyst	Total Acidity Amount of desorbed NH_3 ($mmol \cdot g^{-1}$)	Density of acid sites (10^{-4} $mmol \cdot m^{-2}$)
ZrO_2	1.90	211.13
SO_3H-ZrO_2	0.57	204.46
Al-SBA-15	0.15	4.98
SO_3H-SBA-15	0.16	19.09
H-ZSM-5	12.75	315.78
SO_3H-ZSM-5	6.43	215.71

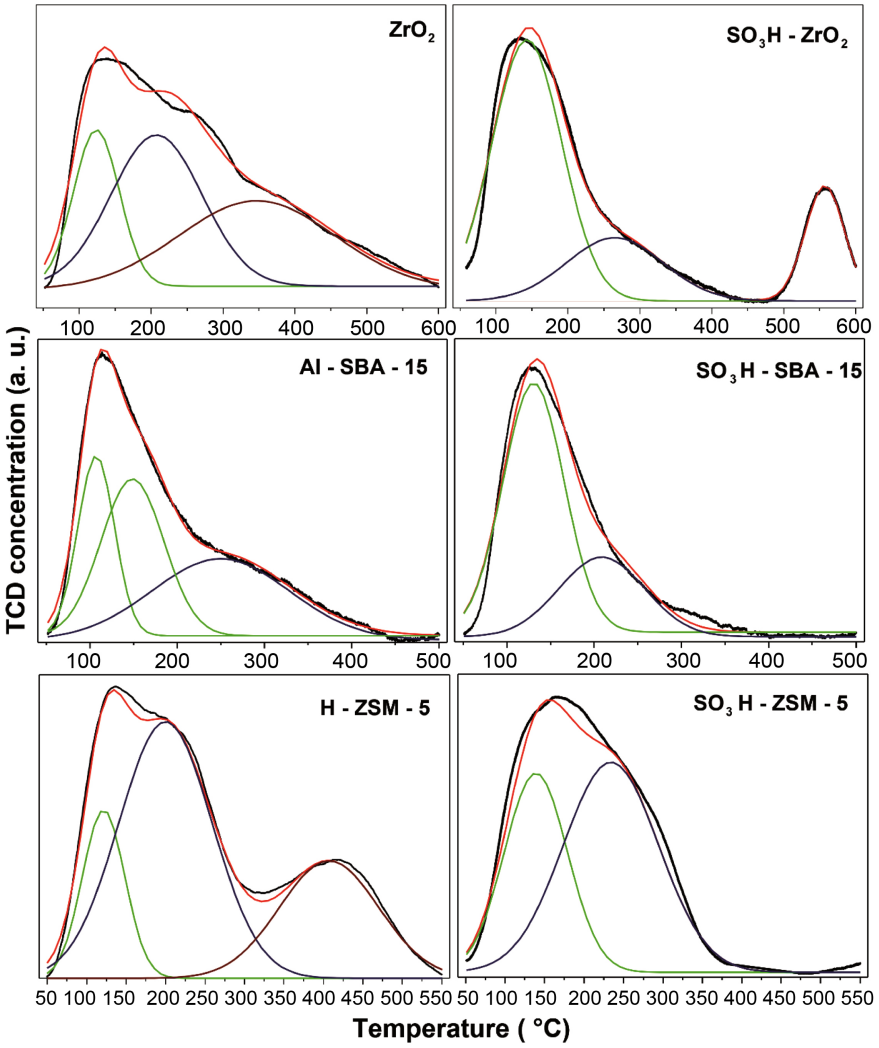

Figure 7. NH_3-TPD spectra of the catalysts.

the case of Al-SBA-15 to 0.05 $mmol \cdot g^{-1}$ for the sulfonated solid SO_3H-SBA-15 and finally from 7.91 $mmol \cdot g^{-1}$ to 4.17 $mmol \cdot g^{-1}$ for H-ZSM-5 and SO_3H-ZSM-5 respectively. It is also important to note that the comparative study between the

three used supports shows that the number of acid sites of medium strength is much higher in the case of zeolite.

Regarding the weak acidity, we note that the number of weak acid sites drops after sulfonation when zirconia is used as a support (mmol·g^{-1}). However, it increases for the other two supports. Indeed, the quantity of desorbed NH_3 goes from 0.37 for ZrO_2 to 0.22 mmol·g^{-1} for SO_3H-ZrO_2. Furthermore, it increases from 0.07 mmol·g^{-1} for Al-SBA-15 to 0.11 mmol·g^{-1} for SO_3H-SBA-15 and from 1.84 mmol·g^{-1} to 2.26 mmol·g^{-1} for HZSM-5 and SO_3H-ZSM-5 respectively.

3.2. Catalytic Performances

Figure 8 shows the hemicellulose conversion after two hours of catalytic test, using the different catalysts. Before their modification with sulfonate groups, the three supports used reveal almost the same conversion of hemicellulose. Indeed, ZrO_2, Al-SBA-15 and H-ZSM-5 solids show conversions of 58.1%, 58.6% and 56.9% respectively, despite they have different structures, specific surface areas, pore structures, pore sizes and acidities. It is important to note that XRD results prove that zirconia simultaneously develops the tetragonal and monoclinic crystallographic phases and Al-SBA-15 possesses a well-ordered hexagonal mesoporous structure indicating 2-dimensional network. Also, H-ZSM-5 exposes a highly crystalline orthorhombic MFI type framework of the zeolite. The N_2 adsorption-desorption results show that H-ZSM-5 has the most developed specific surface area and ZrO_2 has the highest pore size. However, the zirconia support has the highest amount and density of acid sites.

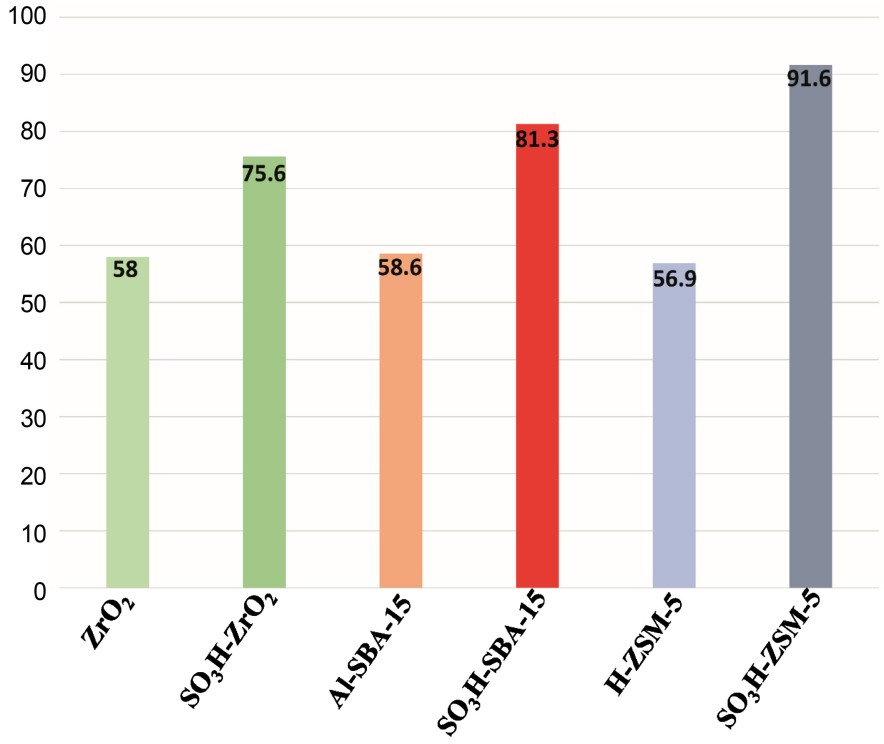

Figure 8. The hemicellulose conversions of the different samples (%).

Furthermore, the incorporation of sulfonate species on the surface of the supports considerably improves the conversion during the hemicellulose hydrolysis reaction. Indeed, SO_3H-ZrO_2, SO_3H-SBA-15 and SO_3H-ZSM-5 show better results than ZrO_2, Al-SBA-15 and H-ZSM-5 supports, respectively. The impregnated solids SO_3H-ZrO_2, SO_3H-SBA-15 and SO_3H-ZSM-5 exhibit hemicellulose conversions of 75.6%, 81.3% and 91.6% respectively. This result seems to correlate perfectly with those obtained by N_2 adsorption-desorption which show that the specific surface areas of the sulfonated catalysts are in the following order SO_3H-ZrO_2 < SO_3H-SBA-15 < SO_3H-ZSM-5.

The analysis of the structural properties of the studied samples proved that the incorporation of the sulfonate species has no significant effects on the structures of the supports despite it causing an important drop in the specific surface areas. However, TEM micrograph of SO_3H-ZSM-5 sample showed spherical particles obtained by aggregation of several nanoparticles having relatively similar shapes. Nevertheless, in the case of the SO_3H-SBA-15 the TEM image revealed that nanoparticles are arranged in the form of fibers characterized by unidirectional channels. The correlation between the catalytic performances and the acidic properties of the different samples indicates that the less acidic support (SBA-15) seems to lead to the best catalytic performances (Table 3) and also the absence of strong acid sites is favorable for the increase of the catalytic properties (Table 4).

The catalytic hydrolysis of hemicellulose leads to the production of several by-products. The most interesting ones generated are formic acid, acetic acid, lactic acid and xylose. The obtained amounts after the various catalytic tests are collected in Table 5. Formic acid (CH_2O_2) and acetic acid (CH_3COOH) are the smallest molecules produced among those studied. Formic acid is a product obtained in all catalytic test, except the one carried out using SO_3H-SBA-15 sample as a catalyst. Otherwise, the impregnation by sulfonate species increases the

Table 4. Distribution of acid sites according to their strength.

	Weak acidity		Medium acidity		Strong acidity	
Catalysts	Amount of desorbed NH_3 ($mmol{\cdot}g^{-1}$)	Density of acid sites (10^{-4} $mmol{\cdot}m^{-2}$)	Amount of desorbed NH_3 ($mmol{\cdot}g^{-1}$)	Density of acid sites (10^{-4} $mmol{\cdot}m^{-2}$)	Amount of desorbed NH_3 ($mmol{\cdot}g^{-1}$)	Density of acid sites (10^{-4} $mmol{\cdot}m^{-2}$)
ZrO_2	0.37	41.08	0.78	87.25	0.75	82.80
SO_3H-ZrO_2	0.22	78.23	0.20	72.23	0.15	54.00
Al-SBA-15	0.07	2.37	0.08	2.61	---	---
SO_3H-SBA-15	0.11	13.41	0.05	5.68	---	---
H-ZSM-5	1.84	45.66	7.91	195.82	3.00	74.3
SO_3H-ZSM-5	2.26	75.70	4.17	140.01	---	---

Table 5. Amounts of the main products obtained after the catalytic tests.

By-product	Formic acid (10^{-6} µmol)	Acetic acid (10^{-6} µmol)	Lactic acid (10^{-6} µmol)	Xylose (10^{-6} µmol)
ZrO_2	17.20	10.34	---	---
SO_3H-ZrO_2	33.71	23.60	20.86	240.81
AL-SBA-15	36.95	12.67	---	237.25
SO_3H-SBA-15	---	15.44	---	---
H-ZSM-5	33.71	41.30	18.53	---
SO_3H-ZSM-5	36.95	11.45	---	---

quantity of formic acid. Furthermore, the amount of formic acid depends considerably on the type of support. Indeed, we notice that it increases in the following order: ZrO_2 < H-ZSM-5 < AL-SBA-15. This may be due to the density of weak acid sites which evolve in the same order. On the other hand, acetic acid is produced during all catalytic tests. The addition of SO_3H species increased the amount of produced CH_3COOH, except in the case where H-ZSM-5 is used as support. Moreover, lactic acid was detected, only when SO_3H-ZrO_2 and H-ZSM-5 catalysts were used. We also note that SO_3H-ZrO_2 and Al-SBA-15 catalysts led to the formation of xylose ($C_5H_8O_5$), which is the biggest molecule produced among those studied. The analysis of the results in which we gathered in the Table 5 indicates that the incorporation of sulfonate species to ZrO_2 and Al-SBA-15 supports improved the formation of all by-products. Nevertheless, it leads to a drop in the production level of acetic and lactic acids when the H-ZSM-5 support was used.

4. Conclusion

In this study, catalysts based on zirconia, A1-SBA-15 and H-ZSM-5 doped with sulfonate species, were synthesized and characterized. Their catalytic activities were tested in the hydrolysis reaction of hemicellulose assisted by a microwave reactor. ZrO_2, A1-SBA-15 and H-ZSM-5 exhibit similar conversion rates of hemicellulose, although they have different structures, specific surface areas, pore structures, pore sizes and acidities. Furthermore, the incorporation of sulfonates species significantly improves the conversion during the hemicellulose hydrolysis reaction. The activity of the different sulfonated samples is found to be in the following order: SO_3H-ZrO_2 < SO_3H-SBA-15 < SO_3H-ZSM-5 and agree with the textural properties of the different solids which show that the specific surface areas of the sulfonated catalysts follow the same order. The correlation between the catalytic performances and the acidic properties of the different samples indicates that the best conversions were obtained with the least acidic solids and especially when the density of strong acid sites decreases.

Conflicts of Interest

The authors declare no conflicts of interest regarding the publication of this paper.

References

[1] González Martínez, M., Ohra-aho, T., Tamminen, T., Da Silva Perez, D., Campargue, M. and Dupont, C. (2019) Detailed Structural Elucidation of Different Lignocellulosic Biomass Types Using Optimized Temperature and Time Profiles in Fractionated Py-GC/MS. *Journal of Analytical and Applied Pyrolysis*, **140**, 112-124. https://doi.org/10.1016/j.jaap.2019.02.011

[2] Ramachandran, K. (2013) Recent Developments for Biodiesel Production by Ultrasonic Assist Transesterification Using Different Heterogeneous Catalyst: A Review. *Renewable and Sustainable Energy Reviews*, **22**, 410-418. https://doi.org/10.1016/j.rser.2013.01.057

[3] Santibáñez, L., Henríquez, C., Corro-Tejeda, R., Bernal, S., Armijo, B. and Salazar, O. (2021) Xylooligosaccharides from Lignocellulosic Biomass: A Comprehensive Review. *Carbohydrate Polymers*, **251**, Article ID: 117118. https://doi.org/10.1016/j.carbpol.2020.117118

[4] Gavilà, L., Constantí, M. and Medina, F. (2015) D-Lactic Acid Production from Cellulose: Dilute Acid Treatment of Cellulose Assisted by Microwave Followed by Microbial Fermentation. *Cellulose*, **22**, 3089-3098. https://doi.org/10.1007/s10570-015-0720-1

[5] Houfani, A.A., Anders, N., Spiess, A.C., Baldrian, P. and Benallaoua, S. (2020) Insights from Enzymatic Degradation of Cellulose and Hemicellulose to Fermentable Sugars—A Review. *Biomass and Bioenergy*, **134**, Article ID: 105481. https://doi.org/10.1016/j.biombioe.2020.105481

[6] Mussatto, S.I., Fernandes, M., Milagres, A.M.F. and Roberto, I.C. (2008) Effect of Hemicellulose and Lignin on Enzymatic Hydrolysis of Cellulose from Brewer's Spent Grain. *Enzyme and Microbial Technology*, **43**, 124-129. https://doi.org/10.1016/j.enzmictec.2007.11.006

[7] Liu, Z., Shi, E., Ma, F. and Jiang, K. (2021) An Integrated Biorefinery Process for Co-Production of Xylose and Glucose Using Maleic Acid as Efficient Catalyst. *Bioresource Technology*, **325**, Article ID: 124698. https://doi.org/10.1016/j.biortech.2021.124698

[8] Kim, J.-H., Choi, J.-H., Kim, J.-C., Jang, S.-K., Kwak, H.W., Koo, B. and Choi, I.-G. (2021) Production of Succinic Acid from Liquid Hot Water Hydrolysate Derived from Quercus Mongolica. *Biomass and Bioenergy*, **150**, Article ID: 106103. https://doi.org/10.1016/j.biombioe.2021.106103

[9] Stoffel, R.B., Neves, P.V., Felissia, F.E., Ramos, L.P., Gassa, L.M. and Area, M.C. (2017) Hemicellulose Extraction from Slash Pine Sawdust by Steam Explosion with Sulfuric Acid. *Biomass and Bioenergy*, **107**, Article ID: 93101. https://doi.org/10.1016/j.biombioe.2017.09.019

[10] Hui, W., Zhou, Y., Dong, Y., Cao, Z.-J., He, F.-Q., Cai, M.-Z. and Tao, D.-J. (2019) Efficient Hydrolysis of Hemicellulose to Furfural by Novel Superacid SO_4H-Functionalized Ionic Liquids. *Green Energy & Environment*, **4**, 49-55. https://doi.org/10.1016/j.gee.2018.06.002

[11] Ormsby, R. (2012) Hemicellulose Hydrolysis Using Solid Acid Catalysts Generated from Biochar. *Catalysis Today*, **190**, 89-97.

https://doi.org/10.1016/j.cattod.2012.02.050

[12] Carà, P. D., Pagliaro, M., Elmekawy, A., Brown, D.R. Verschuren, P., Shiju, N.R. and Rothenberg, G. (2013) Hemicellulose Hydrolysis Catalysed by Solid Acids. *Catalysis Science & Technology*, **3**, Article 2057. https://doi.org/10.1039/c3cy20838a

[13] Wan, L. (2021) Hydrolysis of Corncob Hemicellulose by Solid Acid Sulfated Zirconia and Its Evaluation in Xylitol Production. *Applied Biochemistry and Biotechnology*, **193**, 205-217.

[14] Lai, D., Deng, L., Guo, Q. and Fu, Y. (2011) Hydrolysis of Biomass by Magnetic Solid Acid. *Energy & Environmental Science*, **4**, 3545-3551. https://doi.org/10.1039/c1ee01526e

[15] Yunpu, W., Leilei, D., Liangliang, F., Shaoqi, S., Yuhuan, L. and Roger, R. (2016) Review of Microwave-Assisted Lignin Conversion for Renewable Fuels and Chemicals. *Journal of Analytical and Applied Pyrolysis*, **119**, 104-113. https://doi.org/10.1016/j.jaap.2016.03.011

[16] Ha, S.H., Mai, N.L., An, G. and Koo, Y.-M. (2011) Microwave-Assisted Pretreatment of Cellulose in Ionic Liquid for Accelerated Enzymatic Hydrolysis. *Bioresource Technology*, **102**, 1214-1219. https://doi.org/10.1016/j.biortech.2010.07.108

[17] Ríos-González, L.J., Medina-Morales, M.A., Rodríguez-De la Garza, J.A., Romero-Galarza, A., Medina, D.D. and Morales-Martínez, T.K. (2021) Comparison of Dilute Acid Pretreatment of Agave Assisted by Microwave versus Ultrasound to Enhance Enzymatic Hydrolysis. *Bioresource Technology*, **319**, Article ID: 124099. https://doi.org/10.1016/j.biortech.2020.124099

[18] Desai, N.C., Bhatt, K., Jadeja, D.J., Mehta, H.K., Khedkar, V.M. and Sarkar, D. (2022) Conventional and Microwave-Assisted Organic Synthesis of Novel Antimycobacterial Agents Bearing Furan and Pyridine Hybrids. *Drug Development Research*, **83**, 416-431. https://doi.org/10.1002/ddr.21872

[19] Nain, S., Singh, R. and Ravichandran, S. (2019) Importance of Microwave Heating in Organic Synthesis. *Advanced Journal of Chemistry-Section A*, **2**, 94-104. https://doi.org/10.29088/SAMI/AJCA.2019.2.94104

[20] Wang, X., Li, H., Lin, Q., Li, R., Li, W., Wang, X., Peng, F. and Ren, J. (2019) Efficient Catalytic Conversion of Dilute-Oxalic Acid Pretreated Bagasse Hydrolysate to Furfural Using Recyclable Ironic Phosphates Catalysts. *Bioresource Technology*, **290**, Article ID: 121764. https://doi.org/10.1016/j.biortech.2019.121764

[21] Wang, X., Zhang, C., Lin, Q., Cheng, B., Kong, F., Li, H. and Ren, J. (2018) Solid Acid-Induced Hydrothermal Treatment of Bagasse for Production of Furfural and Levulinic Acid by a Two-Step Process. *Industrial Crops and Products*, **123**, 118-127. https://doi.org/10.1016/j.indcrop.2018.06.064

[22] Agirrezabal-Telleria, I., Requies, J., Güemez, M.B. and Arias, P.L. (2014) Dehydration of D-Xylose to Furfural Using Selective and Hydrothermally Stable Arenesulfonic SBA-15 Catalysts. *Applied Catalysis B-environmenta*, **145**, 34-42. https://doi.org/10.1016/j.apcatb.2012.11.010

[23] Zhang, J., Zhuang, J., Lin, L., Liu, S. and Zhang, Z. (2012) Conversion of D-Xylose into Furfural with Mesoporous Molecular Sieve MCM-41 as Catalyst and Butanol as the Extraction Phase. *Biomass and Bioenergy*, **39**, 73-77. https://doi.org/10.1016/j.biombioe.2010.07.028

[24] Xia, Q., Peng, H., Zhang, Y., Fu, G., Liu, Y., Xiao, Z., Huang, L. and Bi, H. (2021) Microwave-Assisted Furfural Production from Xylose and Bamboo Hemicellulose in a Biphasic Medium. *Biomass Conversion and Biorefinery*. https://doi.org/10.1007/s13399-021-01870-7

[25] Gallo, J.M.R., Bisio, C., Gatti, G., Marchese, L. and Pastore, H.O. (2010) Physicochemical Characterization and Surface Acid Properties of Mesoporous [Al]-SBA-15 Obtained by Direct Synthesis. *Langmuir*, **26**, 5791-5800. https://doi.org/10.1021/la903661q

[26] Ibrahim, M.M., Mahmoud, H.R., El-Molla, S.A. (2019) Influence of Support on Physicochemical Properties of ZrO_2 Based Solid Acid Heterogeneous Catalysts for Biodiesel Production. *Catalysis Communications*, **122**, 10-15. https://doi.org/10.1016/j.catcom.2019.01.008

[27] Ben Nsir, S., Younes, M.K., Rives, A. and Ghorbel, A. (2017) Characterization and Reactivity of Zirconia-Doped Phosphate Ion Catalyst Prepared by Sol-Gel Route and Mechanistic Study of Acetic Acid Esterification by Ethanol. *Journal of Sol-Gel Science and Technology*, **84**, 349-360. https://doi.org/10.1007/s10971-017-4509-6

[28] Ben Hammouda, L. and Ghorbel, A. (2019) Influence of the Zirconium Precursor on the Acidic and Catalytic Properties of Sulfated Zirconia Catalysts Prepared by Sol-Gel Process. *Journal of Sol-Gel Science and Technology*, **89**, 543-552. https://doi.org/10.1007/s10971-018-4877-6

[29] Saravanamurugan, S., Sujandi Prasetyanto, E.A. and Park, S.-E. (2008) Liquid-Phase Reaction of 2'-Hydroxyacetophenone and Benzaldehyde over SO_3H-SBA-15 Catalysts: Influence of Microwave and Thermal Effects. *Microporous and Mesoporous Materials*, **112**, 97-107. https://doi.org/10.1016/j.micromeso.2007.09.013

[30] Lai, S., Meng, D., Zhan, W., Guo, Y., Guo, Y., Zhang, Z. and Lu, G. (2015) The Promotional Role of Ce in Cu/ZSM-5 and *in Situ* Surface Reaction for Selective Catalytic Reduction of NO_x with NH_3. *RSC Advances*, **5**, 90235-90244. https://doi.org/10.1039/C5RA12505G

[31] He, X., Chen, Y., Liu, Y., Fang, L., Chen, Z. and Ji, H. (2019) Distribution of Products from Catalytic Conversion of Cellulose over Metal-Modified Hierarchical H-ZSM-5 in Aqueous Media. *Catalysis Letters*, **149**, 2078-2088. https://doi.org/10.1007/s10562-019-02795-7

[32] Prinsen, P., Luque, R. and González-Arellano, C. (2018) Zeolite Catalyzed Palmitic Acid Esterification. *Microporous and Mesoporous Materials*, **262**, 133-139. https://doi.org/10.1016/j.micromeso.2017.11.029

[33] Zhao, J.-P., Cao, J.-P., Wei, F., Zhao, X.-Y., Feng, X.-B., Huang, X., Zhao, M. and Wei, X.-Y. (2019) Sulfation-Acidified HZSM-5 Catalyst for *in-Situ* Catalytic Conversion of Lignite Pyrolysis Volatiles to Light Aromatics. *Fuel*, **255**, Article ID: 115784. https://doi.org/10.1016/j.fuel.2019.115784

[34] Shi, G., Yu, F., Yan, X. and Li, R. (2017) Synthesis of Tetragonal Sulfated Zirconia via a Novel Route for Biodiesel Production. *Journal of Fuel Chemistry and Technology*, **45**, 311-316. https://doi.org/10.1016/S1872-5813(17)30019-1

[35] Cabrera-Munguia, D.A., González, H., Tututi-Ríos, E., Gutiérrez-Alejandre, A. and Rico, J.L. (2018) Acid Properties of M-SBA-15 and M-SBA-15-SO_3 H (M = Al, Ti) Materials and Their Role on Esterification of Oleic Acid. *Journal of Materials Research*, **33**, 3634-3645. https://doi.org/10.1557/jmr.2018.374

[36] Xing, S., Lv, P., Fu, J., Wang, J., Fan, P., Yang, L. and Yuan, Z. (2017) Direct Synthesis and Characterization of Pore-Broadened Al-SBA-15. *Microporous and Mesoporous Materials*, **239**, 316-327. https://doi.org/10.1016/j.micromeso.2016.10.018